IEEE Access
Multidisciplinary | Rapid Review | Open Access Journal

Received April 28, 2020, accepted June 18, 2020, date of publication June 22, 2020, date of current version July 7, 2020.

Digital Object Identifier 10.1109/ACCESS.2020.3004141

A Wavelet Based Deep Learning Method for Underwater Image Super Resolution Reconstruction

YUZHANG CHEN, KANGLI NIU, ZHANGFAN ZENG, AND YONGCAI PAN, (Fellow, IEEE)
School of Computer Science and Information Engineering, Hubei University, Wuhan 430062, China

Corresponding author: Yuzhang Chen (hubucyz@foxmail.com)

This work was supported in part by the General program of Natural Science Foundation of Hubei Province under Grant 2019CFB733, and in part by the Innovation and Entrepreneurship Training Program for College Students in Hubei Province under Grant 201710512051 and Grant S201910512024.

ABSTRACT In order to solve the scattering degradation by turbulence and suspended particles in underwater imaging, traditional processing methods including image enhancement, restoration and reconstruction have been continuously researched. But most of them rely on degradation models, and there exist problems of ill-posed. Image super resolution reconstruction based on deep learning has become a hot topic in recent years. In order to further improve the effectiveness and efficiency of deep learning based methods, an improved image super-resolution reconstruction algorithm based on deep convolutional neural network is proposed in this paper. The wavelet basis which can effectively simulate the waveform and characteristics of underwater turbulence is selected to replace the neuron fitting function in order to improve the accuracy and efficiency of the algorithm. An improved dense block structure (IDB) is introduced into the network which can effectively solve the gradient disappearance problem of deep convolutional neural network and improve the training speed at the same time. The method proposed in this paper has been verified in laboratory flume, public data set and real water body. The experimental results show that under the same conditions, the proposed algorithm shows improvements on various evaluation parameters compared with DRFN, VDSR and DRCN method. So it can be concluded that the proposed method can effectively improve the quality of deep learning based reconstruction for imaging in natural water.

INDEX TERMS Convolutional neural network, super-resolution, signal to noise ratio, underwater image.

I. INTRODUCTION

Imaging detection is an important research topic in marine military, underwater resource development and environmental monitoring. According to previous studies, the serious degradation of underwater image quality is caused by the absorption and scattering of light, suspended particles, turbulence distortion and so on, among which turbulence degradation is the most serious problem in natural waters. Optimizing image enhancement algorithms by setting up a degradation model is an effective way to improve the image quality on the basis of maintaining the cost of hardware.

Traditional underwater image processing methods include image enhancement and restoration algorithms [1]–[4]. In recent years, scholars have introduced various mathematical methods such as estimation [5]–[8], fusion [9], color correction [10]–[12], and the combination of depth neural network [13]–[15] to optimize the quality of underwater image restoration and reconstruction. Hou *et al.* [16]–[20] considered the damage of scattering and optical turbulence to underwater imaging, established a degradation model of underwater imaging, and analyzed the influence of suspended particles, turbulence, and path scattering on underwater optical imaging. Nootz *et al.* [21]–[23] established laboratory and field underwater turbulence experimental system, and analyzed the influence of optical turbulence on the resolution of underwater imaging system through field measurement. Matt *et al.* [24], [25] established a turbulent environment experimental platform with variability and reproducibility. The fluid field was analyzed by Doppler velocimeter and particle image velocimetry (PIV) system, and the measurement results were compensated by computational fluid

The associate editor coordinating the review of this manuscript and approving it for publication was Zhan-Li Sun.

dynamics model. Farwell *et al.* [26], [27] studied the intensity and coherent distribution of turbulence in underwater beam propagation based on the power spectrum model of ocean turbulence.

However, some common problems of above algorithms are as following: (1) The relationship between noise reduction and contrast enhancement cannot be well handled, which leads to inadequate noise elimination or damaged details in reconstructed images. (2) Digital images are mostly two-dimensional or three-dimensional digital matrices, the amount of data is very large, and the iteration time of the algorithm is too long to achieve real-time performance. Therefore, the classical method of underwater image processing cannot get high-quality underwater image restoration results quickly and accurately. (3) The problem of low efficiency and dependence on models limit the application scope and real-time performance.

Therefore, it is very necessary and urgent to find a fast and effective method to process underwater image, so as to obtain images with high signal-to-noise ratio and good clarity in real-time underwater imaging. Since the rapid development of super-resolution reconstruction technology based on deep learning in recent years, this paper innovatively introduces it into underwater image restoration to improve the quality of underwater image.

In recent years, image super-resolution reconstruction based on deep learning has become a research hotspot. Shen *et al.* [28]–[30] proposed a super-resolution reconstruction algorithm for MODIS remote sensing images, and made contributions to adaptive norm selection for regularized image restoration and super-resolution. Lim *et al.* [31] proposed EDSR method. The most significant improvement is the removal of redundant SRResNet modules so that the size of the model could be expanded to improve the quality of the results. With the same computing resources, EDSR can stack more network layers or extract more features from each layer to get better performance. Wang *et al.* [32] proposed SFTGAN method, using the image segmentation mask as the prior feature condition of the super-resolution and the prior category information to solve the problem of the unreal super-resolution texture and to restore the real super-resolution texture of the image through the depth space feature transformation. Zhang *et al.* [33] put forward RankSRGAN method and optimized SR model for perception index. They introduced ''Ranker'' to learn the behavior of perceptual indicators through ranking learning. RankSRGAN could combine the advantages of different SR methods to achieve the best performance in perception metrics and restore more realistic texture.

However, the common image super-resolution algorithms are ''blind'' to image processing, which means that the algorithm does not know the defects of the images. Generally, the underwater image is most seriously affected by turbulence. Because of the flexible transformation property of wavelet base, it can simulate the wave form and characteristics of turbulence well and reflect the randomness of turbulence. Therefore, in this paper, a deep convolution neural network based on wavelet transform is proposed to do the training of the mapping relationship, and an improved dense block structure (IDB) is also proposed to solve the gradient disappearance problem of deep convolutional neural network and improve the training speed at the same time.

II. THEORY

With the gradual development of underwater imaging devices, turbulence is the bottleneck obstacle to overcome the imaging degradation in natural waters. Turbulence is a complex and irregular state of motion of fluid. Most of the ocean and river are in this random state of motion.

Wavelet is a short-term signal whose energy is concentrated in a short period of time. It can effectively simulate the waveform and characteristics of turbulence and retain the edge information of image. When it is used in neural network, it can make the extraction of image information more accurate and efficient. The two-dimensional discrete wavelet transform is used to transform the discrete image data into coefficients in the wavelet domain. The image data are filtered by selecting a reasonable threshold, and then the desired target image is obtained by inverse wavelet transform. The multi-resolution characteristic of wavelet transform is beneficial to the protection of image edge details and feature extraction. Wavelet bases can be selected flexibly according to different practical problems, and the corresponding processing effect can be obtained.

A. WAVELET RECONSTRUCTION FUNCTION

Hussain decomposes turbulence signals into

$$f(x,t) = \overline{f}(x) + f_c(x,t) + f_r(x,t) \tag{1}$$

where $\overline{f}(x)$ represents the average time, f_c and f_r denotes the coherent and the incoherent part of the turbulent structure, among which the energy of turbulence signal is concentrated in coherent structure. Therefore, the coherent structure of turbulence plays an important role in understanding the generation and change of turbulence.

The continuous wavelet transform of a signal $x(t) \in L^2(R)$ can be expressed as:

$$X_\omega(a,b) = \frac{1}{\sqrt{|a|}} \int_{-\infty}^{+\infty} x(t)\psi\left(\frac{t-b}{a}\right)dt \tag{2}$$

Its reconstruction (inverse transformation) formula is as follows:

$$X(t) = \int_0^{+\infty} \int_{-\infty}^{+\infty} \frac{1}{a^2} X_\omega(a,b) \frac{1}{\sqrt{|a|}} \psi\left(\frac{t-b}{a}\right) dadb \tag{3}$$

where a is the scale factor that decides the scaling scale of the wavelet. In signal processing, a is used to control the frequency of the wavelet. b is a translation factor which can delay the wavelet signal to the region of interest in the analysis. The wavelet bases for translation and scaling is:

$$\psi_{a,b}(t) = \frac{1}{\sqrt{|a|}} \psi\left(\frac{t-b}{a}\right), \quad a, b \in R, a \neq 0 \tag{4}$$

Due to its good autocorrelation performance and low cross-correlation, orthogonal Harr wavelet and Morlet wavelet are used for reconstruction in order to distinguish adjacent harmonics effectively. The coherent structures of turbulence at specific scales a and b can be obtained by:

$$X(t,a)=\int_{-\infty}^{+\infty}\frac{1}{H_{\psi_1\psi_2}}\left[\left(W_{\psi_1}X\left(t\right)\right)\left(b,a\right)\right]\psi_{2a,b}\left(t\right)\frac{1}{a}db \tag{5}$$

where ψ_1 is Morlet wavelet, ψ_2 is Harr wavelet, $H_{\psi_1\psi_2}$ is a constant related only to the selected wavelet basis. So as long as the specific scale is determined, the coherent structure of turbulence can be reconstructed.

B. IMAGE SUPER RESOLUTION RECONSTRUCTION BASED ON WAVELET DEEP CONVOLUTION NEURAL NETWORK

The structure of the improved deep intensive convolution neural network designed in this paper is shown in Figure. 1.

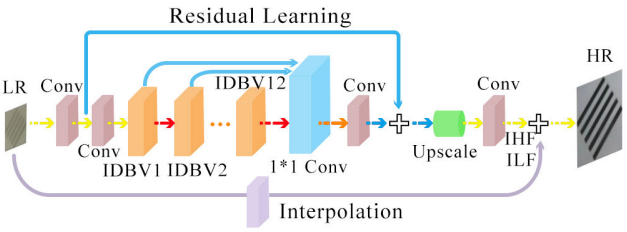

FIGURE 1. Structure of the wavelet deep convolution neural network.

The improved network consists of two main parts:

$$I(X)=A(X)+B(X) \tag{6}$$

where LR is the low-resolution image, HR is the high-resolution image, $I(X)$ is the final reconstructed image, X is the captured low resolution image, $A(X)$ is the low-frequency part of the image, which is obtained by bi-cubic interpolation of low-resolution image, $B(X)$ is the high-frequency part of the image, which represents the output image processed by deep convolution neural network. As the low-frequency information carried by the low-resolution image is similar to the low-frequency information of the high-resolution image, it takes a lot of time to carry this part in training. So, we only need to study the high-frequency residual between the high-resolution image and the low-resolution image. Thus the network constructed in this paper can effectively avoid repeated learning of low-frequency part, thus speeding up the convergence of the model.

Figure 1 shows the deep convolution neural network applied to learning the high-frequency part of image information. It consists of four parts, including convolution layer for learning low-level features, which contains two Conv convolution layers; improved dense blocks for learning high-level features including 12 IDBs; the fusion layer used to fuse the intensive features of learning; reconstructed blocks for generating high frequency features, including an upper sampling layer and a convolution layer.

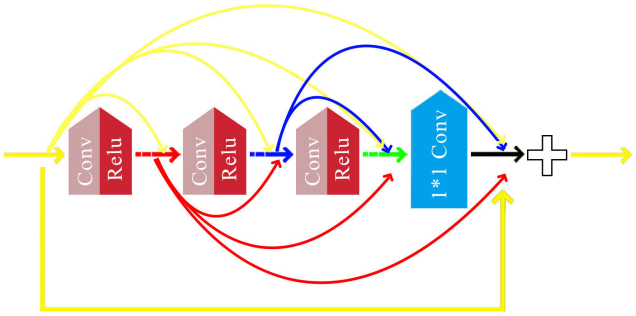

FIGURE 2. Schematic structure of improved dense block (IDB).

The output of neural network can be expressed by:

$$B'(X)=Ac(\sum_{i\in M_j}x_i^{l-1}\times a_{ij}^l+b_j^l) \tag{7}$$

where x_i denotes the values of the pixels in the feature graph, l is the number of the convolution layer, i and j are the position of the pixels, Ac is the activation function for the neural network, M is the convolution core, a and b are the weights and constant biases in the convolution core respectively, which are set as scale factor and shift factor of the turbulent coherent structure function in Eq.5 respectively.

In the training process, the sample image is first reduced and then enlarged by interpolation. Activation function is used to assist neuron convolution function to describe the modeling process, which is represented by a and b. And loss function is used to modify these two parameters. In the process of neuron convolution, the convolution nucleus is used to partition, and the fitting function of neuron convolution modeling can be expressed by Eq.7. Residual function can be used as loss function, which is guided by the method proposed in VDSR [3]. The image is compensated by zero before each convolution in the convolution neural network proposed in this paper, which ensures that all the feature maps and the final output image are consistent in size, and avoids the problem that the image will become smaller and smaller through gradual convolution. Residual structure connects shallow and deep convolution layers by cross-layer in deep network, making the convolution layer fit for the residual of feature map, which greatly reduces the computational complexity of training process, and also reduces the gradient dispersion phenomenon.

The middle layer of residual network is improved by introducing an improved dense block structure. The input of each layer of the network is the union of the output of all the layers in front of it. And the feature maps learned by that layer will be passed directly to the back of all layers as input. In this paper, an improved dense block structure (IDB) is proposed by combining residual block with dense block structure.

The input low-resolution image is basically consistent with the low-frequency part of the corresponding high-resolution image, which results that the pixel values of the residual image are mostly very small. In order to learn the high

frequency part end-to-end mapping function F, the idea of residual learning is adopted in the dense convolutional neural network for training high frequency part information. The loss function $H(\lambda)$ of the network model is constructed as:

$$\begin{aligned} \mathrm{H}(\lambda) &= \frac{1}{N}\sum_{i=1}^{N}\left\|(\mathrm{Z}_i - X_i) - F(\lim_{x\to\infty} X_i;\lambda)\right\|^2 \\ &= \frac{1}{N}\sum_{i=1}^{N}\left\|r - F(\lim_{x\to\infty} X_i;\lambda)\right\|^2 \\ \lambda &= \{W_1, W_2, \ldots, W_n, b_1, b_2, \ldots b_n\} \end{aligned} \tag{8}$$

where N is the number of training samples, Z_i is the output high resolution images, X_i is the ith low-resolution input image, r is the residual image information of the standard high-resolution output and low-resolution input.

C. ESTABISHMENT AND TRAINING OF SELF-BUILT DATA SETS

In order to ensure the diversity of experimental data, the images for training were captured in the Yangtze River to form self-built data sets. Like the images in the experiment, the self-built data set is affected by the underwater turbulence. Therefore, the training of self-built data set can make the network learn the information characteristics of underwater image well. Figure 3 A1 and A2 are the images of test targets 1 and 2 in the water of the Yangtze River, and Figure 3 B1 and B2 are the images of test targets 1 and 2 in the clear water. It can be seen that the image quality in clear water is relatively high, and there is basically no noise, while the image in the Yangtze River water contains more noise, and the resolution is very low. In this paper, a large number of datasets for training are collected to solve the difficulty of data acquisition.

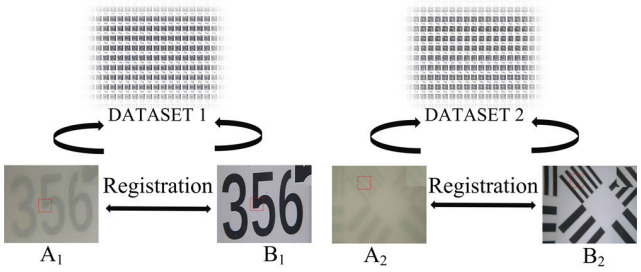

FIGURE 3. Sample images of the self-built data sets.

In order to improve the applicability of the proposed algorithm, a large number of data sets for training were collected. The images before and after degradation of training target were registered to obtain sample training pairs with size of 1064 × 924. The image is first converted into Y-channel from YC_bC_r color space, and then the obtained image is segmented by convolution kernels into 64 × 64 image blocks according to the step size of 10. Then the training set is expanded by rotating and mirroring. The number and size of training, calibration and test images are shown in Table 1. The image blocks collected from these training sets will be used in feature extraction steps, and the convolutional neural network model designed in this paper will be cross-trained.

TABLE 1. Number and size of data set.

Symbol	Training set	Check set	Test set	Test set
Number	19814	2035	100	10
Size	64 x 64	64 x 64	128 x 128	1064 x 924

During the cross-training process, the training set is divided into 10 parts, each round of training will select 9 as the training set data, the remaining one will be used as the test set to adjust the network parameters. Each round of verification set is different, so 10 rounds of cycle constitute cross-training. Through this way, we can effectively select more favorable data sets for network training, so as to prevent the overall effect of the network from being affected by poor performance of some training sets.

The aim of data set training is to find the least summation of the average Euclidean distances between the original high-resolution image and the reconstructed image:

$$W, b = \arg\min_{W,b} \frac{1}{2N}\left\|Z_i - \widehat{Z}_i\right\|_2^2 \tag{9}$$

Peak signal to noise ratio (PSNR) and Structural similarity (SSIM) are the two most widely used indicators to measure the quality of image reconstruction. The former quantitatively calculates the errors between the processed results and the original image. Higher PSNR means less distortion, while the closer the SSIM approaches 1, the better the restored results. Therefore, this paper objectively evaluates the advantages and disadvantages of various reconstruction methods by using these two indicators for laboratory experiments. However, in the field experiments, there is no reference image, PSNR and SSIM cannot be used. So we select the blur metric (BM) [34], [35], grayscale mean gradient (GMG) and Laplacian sum (LS) [34] as the evaluation indexes. The smaller the BM value, the clearer the image, and the higher the GMG and LS values, the higher the image quality.

The BM is defined as follows:

$$\begin{aligned} BM &= \max(sD_{vertical}, sD_{horizontal}), sD_{vertical} \\ &= \sum_{i,j=1}^{m-1,n-1} D_{vertical}(i,j), \\ sD_{horizontal} &= \sum_{i,j=1}^{m-1,n-1} D_{horizontal}(i,j), \\ & i \in (0, m-1), \quad j \in (0, n-1), \\ & \begin{cases} D_{vertical} = |F(i,j) - F(i-1,j)| \\ D_{horizontal} = |F(i,j) - F(i,j-1)| \end{cases} \end{aligned} \tag{10}$$

where $D_{vertical}$ and $D_{horizontal}$ represent different images in the vertical and horizontal directions. $F(i,j)$ is the pixel of

coordinate (i, j) on the image plane, and (m, n) is the size of the image. Then the blur metric can be normalized by the range 0 to 1.

$$GMG = \frac{1}{(M-1)(N-1)} \sum_{i=1}^{M-1} \sum_{j=1}^{N-1} \sqrt{\frac{\alpha^2 + \beta^2}{2}}$$
$$\begin{cases} \alpha = f(x, y+1) - f(x, y) \\ \beta = f(x+1, y) - f(x, y) \end{cases} \tag{11}$$

where $f(x, y)$ denotes the point at coordinate (x, y) on image plane, and (M, N) is the size of the image.

$$LS = \frac{\sum_{i=1}^{M-1} \sum_{j=1}^{N-1} \left| \begin{array}{l} 8 \times f(x, y) - f(x, y-1) - f(x-1, y) - \\ f(x+1, y) - f(x, y+1) - \\ f(x-1, y-1) - f(x-1, y+1) - \\ f(x+1, y-1) - f(x+1, y+1) \end{array} \right|}{(M-2)(N-2)}$$

where $f(x, y)$ denotes the point at coordinate (x, y) on the image plane, (M, N) is the size of image.

III. FIELD TESTS AND EXPERIMENTAL RESULTS

The training platform of algorithm is: the operating system is Ubuntu 14.04 (Canonical Ltd, London, England), the CPU is Core i7–9700K (Quad–core 4.9 GHz) (2200 Mission College Blvd. Santa Clara, CA 95054–1549 USA), and the graphics card is ASUS DUAL RTX2070–O8G–EVO (ASUS, Taipei City, Taiwan). The programming is performed in Anaconda (Austin, Texas, USA). If the computer configuration is lowered or improved, the algorithm time will increase or decrease accordingly.

The captured image sequences are processed and compared by the proposed algorithm along with MAP-regularized robust reconstruction for underwater imaging detection (ROBUST) [1], Deep Recurrent Fusion Network for Single-Image Super-Resolution With Large Factors (DRFN) [2], Accurate Image Super-Resolution Using Very Deep Convolutional Networks (VDSR) [3], Deeply-Recursive Convolutional Network for Image Super-Resolution (DRCN) [4], the codes of which are obtained from the author's project code's open web page.

The network structure parameters are shown in Table 2, where ''Kernel size'' is the size of convolution kernel, ''Padding'' is the number of layers of each input edge supplemented by 0, and ''Bias'' is whether to add bias.

TABLE 2. Table of network structure parameters.

Part	*	Layer	Kernel size	Padding	Bias
Part 1	1	Conv	3	1	True
	2	Conv	3	1	True
Part 2	IDB1	Conv	3	1	False
		Conv	3	1	False
		Conv	3	1	False
		Conv	1	0	False
	...	...	...	...	...
	IDB12	Conv	3	1	False
		Conv	3	1	False
		Conv	3	1	False
		Conv	1	0	False
Part 3	1	Conv	1	0	True
	2	Conv	3	1	True
Part 4	1	Deconv	3	1	True
	2	Conv	3	1	True

A. LABORATORY EXPERIMENTS

In this paper, the experimental system of underwater turbulence is established with 532 nm green semiconductor laser as the light source; high-speed CMOS image sensor is used to collect images. The laser spot size is 10-20 mm and the power is 200 MW. The experimental water tank is made of acrylic plate with high transmittance. More than 90% of the laser source is irradiated on the target plate. Its size is $150cm \times 34cm \times 33cm$ (length, height and width). The inlet and outlet are all 40mm round holes, and turbulent flow is formed by water pump at different heights. The experimental system uses a circulating pump with a maximum head of 5 meters and a maximum flow of $7.8m^3/h$ to generate fluid power. The laser and sensor are 33 cm from the target plate. In order to reduce the experimental error, the experiment was carried out in dark environment. The three-dimensional structure of the experimental system is shown in Fig. 4.

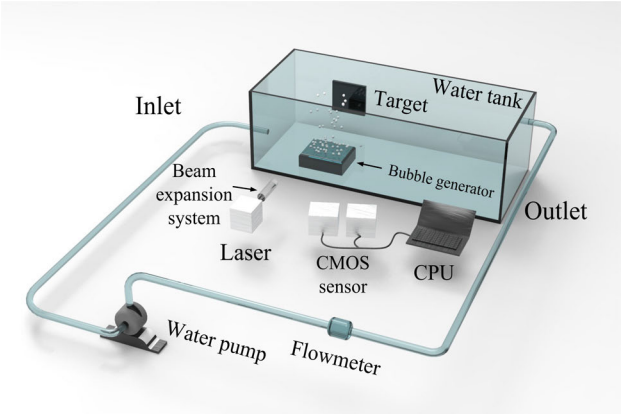

FIGURE 4. Three-dimensional structure of laboratory experiment system.

By controlling the velocity of water flow in the water tank, turbulence of different intensity can be obtained. The flow meter can read the velocity in real time, and then calculate the turbulent Reynolds number and turbulence intensity to ensure that the sample image can be obtained in the turbulent environment. When the water velocity of the intake is $5m/s$, the target object is photographed 60 times by CCD sensor in 5 seconds, which is considered as the micro turbulence environment.

Self-built data sets are used to cross train each algorithm. In the equation 5, a is set as 0.6745 and b as 0.9875. The variances of PSNR during cross-training are shown in Figure 5.

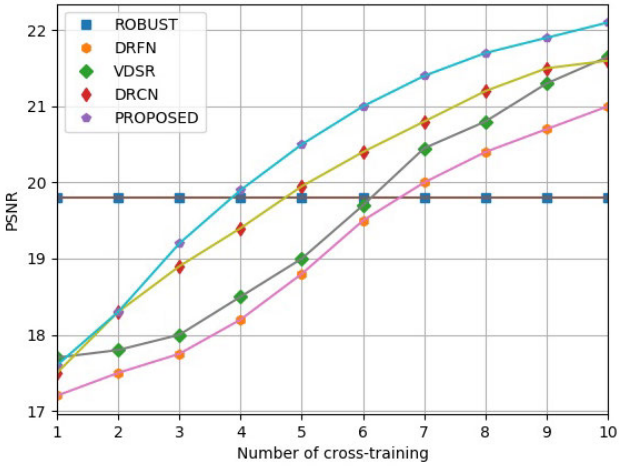

FIGURE 5. The variances of PSNR during cross-training.

It can be seen from the results in the figure that after cross training, the method in this paper has the best effect on self built data set processing.

In this paper, peak signal-to-noise ratio (PSNR) and structure similarity index (SSIM) are selected as evaluation indexes. The collected sample image, reconstructed image of each algorithm, the evaluation value of each image and the running time of each algorithm are shown in Figure 6.

From the perspective of image reconstruction effect, the ROBUST and DRFN methods eliminate a certain degree of blur, but the processing results are darker, and introduce a larger ringing effect. VDSR improves the ringing effect, while the image distortion is not improved. DRCN improves the resolution of the image, while the color of the image is still dark, and the distortion has not been substantially improved. It can be seen that image restoration and reconstruction algorithms have significant effect in improving resolution and de blurring, they cannot effectively correct image distortion. Our proposed method can not only eliminate certain image noise, but also significantly improve image distortion, which shows the efficiency of this algorithm.

According to the evaluation results, the SSIM values of DRCN are larger than those of ROBUST method and DRFN method, but only to a small extent. The SSIM value of the image processed by proposed method is the largest, followed by that of the VDSR-processed one. However, the PSNR value of VDSR method is small, which indicates that the distortion gets worse after image processing.

In terms of run-time, the method proposed in this paper has the shortest time and obvious advantages.

Therefore, the method proposed is superior to the other four methods in reconstruction quality and running speed, which is suitable for underwater detection and related applications in low turbulence state.

In order to compare the effect of adding wavelet basis and IDB to the underwater image processing respectively, we use the above image experiments, and the results are shown in table 3.

TABLE 3. Experimental results of separation of wavelet and IDB.

	With wavelet Without IDB	With IDB Without wavelet	With IDB With wavelet
PSNR	9.7721	8.9623	10.4066
SSIM	0.6670	0.5812	0.6827
Time(s)	5.651968	5.001578	4.958150

The experimental results show that in the case of weak turbulence, the image quality can be greatly improved by using wavelet alone. Using IDB alone can reduce running time of the algorithm. When both of them are used, the image quality of underwater image is the best.

When the inflow velocity reaches 25m / s, it is seen as the strong turbulence environment, and the distortion degree of the image increases greatly. The collected sample image, the result of image restoration and reconstruction, the evaluation value and the running time of each algorithm are shown in Figure 7.

The image reconstruction results in Figure 7 reveal that the traditional DRFN method has no obvious ringing effect, but its image is as fuzzy as the ROBUST method's. The results also show that the VDSR method still causes distortion in the strong turbulence state. However, compared with other images, the reconstruction image of the method proposed has a certain degree of fuzziness, it shows the outline of the stripe in the sample image more clearly, which makes the method more practical in the context of strong turbulence.

According to the evaluation results, the PSNR values of VDSR method are larger than those of ROBUST method and DRFN method. Given strong turbulence, the PSNR value of DRCN method is relatively large, while its SSIM value is small, and the SSIM value of the method proposed in this paper is the largest.

In comparison to other algorithms, the method proposed still has obvious advantages in processing time.

The results show that the method proposed in this paper is superior to other methods in image distortion, which has a greater improvement in image resolution and clarity. In the strong turbulence environment, we separate the wavelet basis and IDB, and the results are shown in Table 4.

TABLE 4. Experimental results of separation of wavelet and IDB.

	With wavelet Without IDB	With IDB Without wavelet	With IDB With wavelet
PSNR	10.7892	9.9623	11.1276
SSIM	0.2437	0.2012	0.2902
Time(s)	5.619566	5.121578	5.042153

The experimental results show that both wavelet basis and IDB can improve the performance of the network in strong or weak turbulence environment, but using them at the same

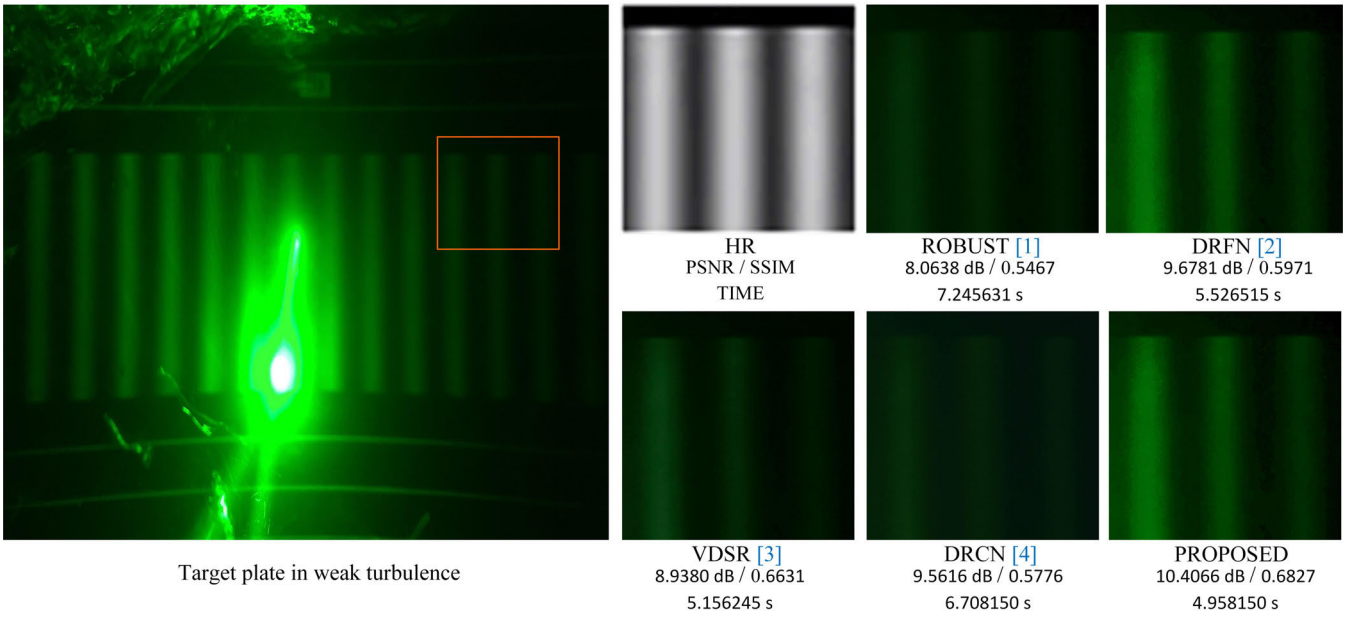

FIGURE 6. Super-resolution result of our method compared with existing algorithms in micro turbulence environment.

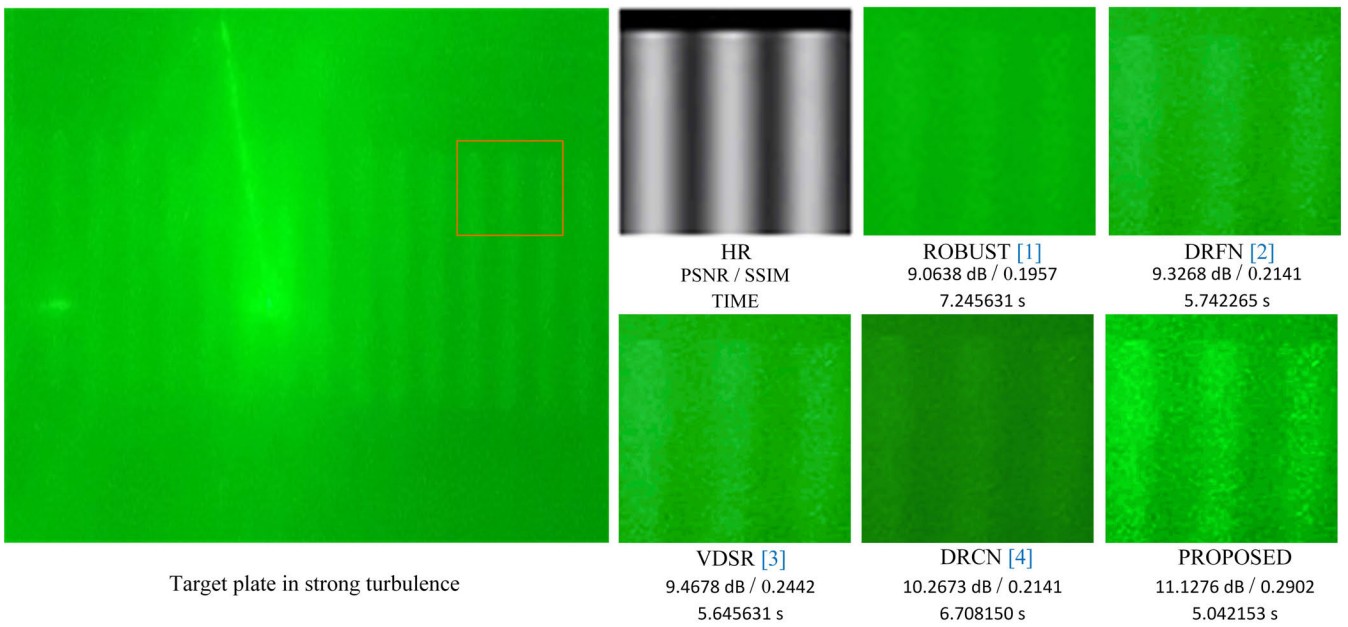

FIGURE 7. Super-resolution result of our method compared with existing algorithms in strong turbulence environment.

time can make the network achieve the best results in underwater image processing.

B. PUBLIC DATASETS EXPERIMENTS

In order to further verify the effectiveness of the algorithm in this paper, we reconstructed images from the milk dataset with turbidity of 15 and the Chlorophyll dataset with turbidity of 21 from the TURBID Dataset [36], and compared with the other algorithms.

The sample images, reconstruction results, evaluation values and running time of each algorithm from the two datasets are shown in Figure 8.

The experimental results demonstrate that the image reconstruction results of the ROBUST method and the DRFN method are relatively poor, while the VDSR method, the DRCN method and the proposed one show better outcomes. In the milk dataset and the Chlorophyll dataset, the method proposed runs better than other methods, because

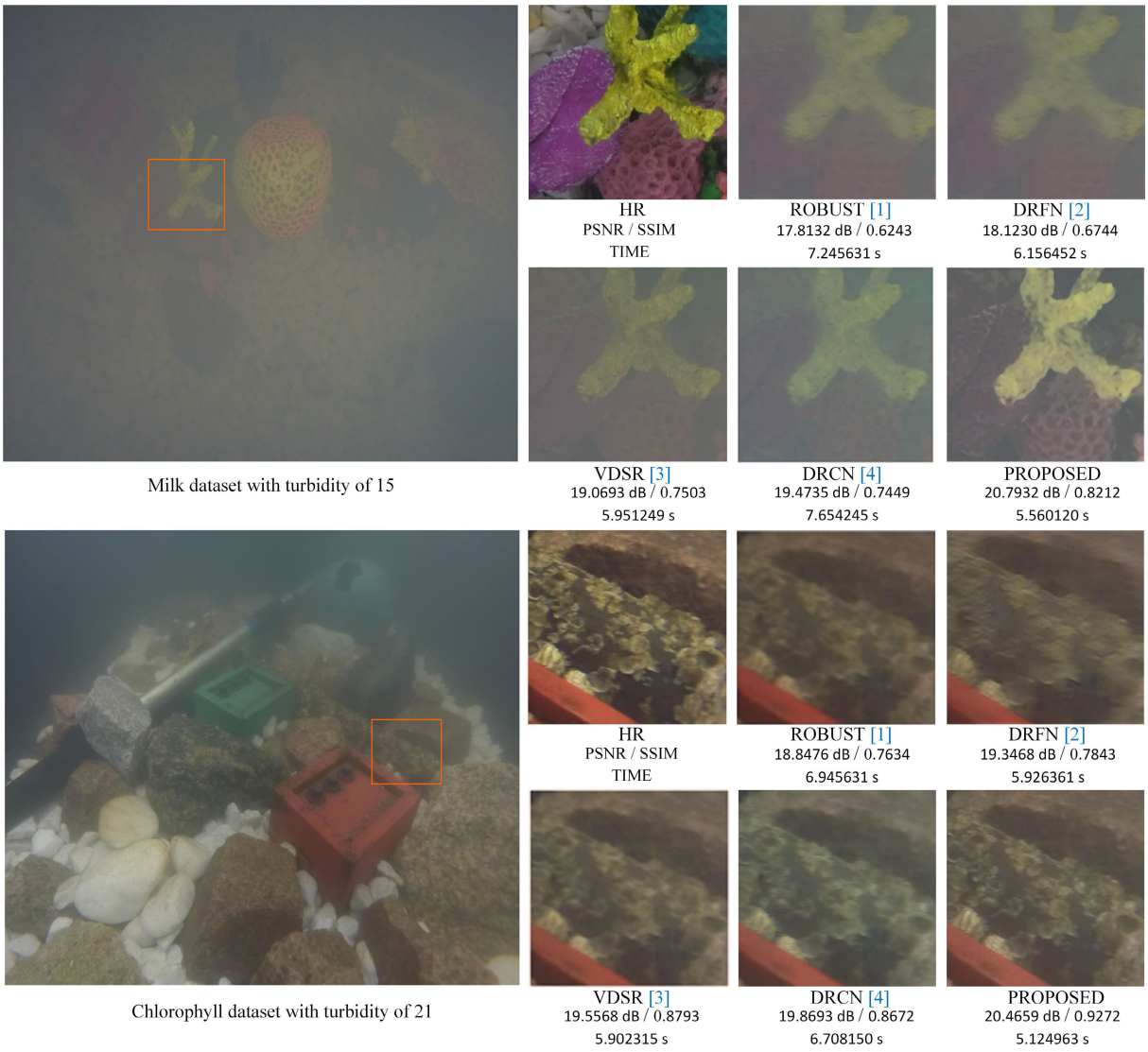

FIGURE 8. Public datasets super-resolution result of our method compared with existing algorithms.

the datasets are mainly generated for turbidity. According to the paper on datasets, the generation of turbidity mainly affects the scattering. Therefore, the robust light scattering model and the light scattering model considering particle scattering will get better recovery effect. In the turbulent state, neither the ROBUST method nor the DRFN method nor the measurement model depending on the measurement parameters can achieve good results.

The method proposed in this paper is applicable to both turbulent and particle scattering conditions, so it is more practical. This method can provide guidance on how to reduce the influence of turbulent environment on underwater imaging.

C. FIELD EXPERIMENTS

Experiments on turbulent water environment in the East Lake, Yangtze River and South China Sea were carried out. The sample image is collected by the underwater packaging

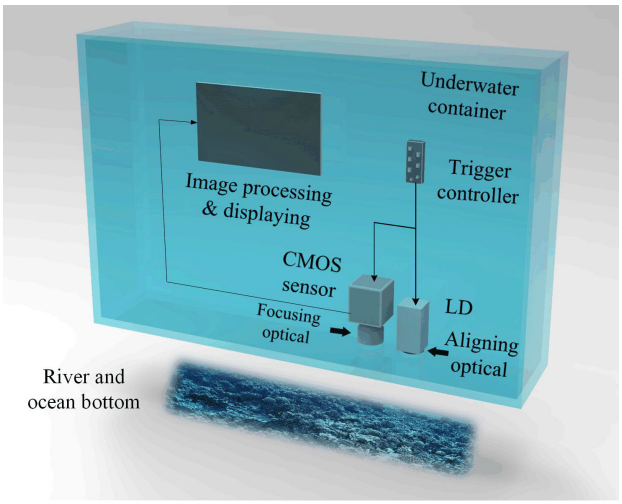

FIGURE 9. Framework of underwater experimental detection system.

FIGURE 10. Super-resolution result of our method compared with existing algorithms in field experiment.

imaging system, as shown in Figure 9. The laser and CMOS image sensors working at 465nm are encapsulated in a water-proof water tank, and the image is transmitted to the image processing module by the image sensor. Table 5 shows the physical characteristics of the experimental system.

TABLE 5. Physical properties of experimental system.

Parameters	Value
Water attenuation (t)	$2.85m^{-1}$
LD power (P_0)	$500mW$
Operating Voltage (V)	$12V$
Angle of viewing (θ)	85^o
Distance between LD and CCD (d_0)	$1cm$

The processing effect of robust method is not very good, so in the field test, we omit the method of robust to carry out the test, and use the other three methods to compare with the method in this paper. The sample image and reconstruction results are shown in Figure 10. Table 6 compares the running time of each algorithm.

TABLE 6. Run-time of each algorithm in field experiment.

TIME	DRFN	VDSR	DRCN	**Proposed**
Img1	6.563124	5.814561	6.874562	**5.023651**
Img2	6.567113	6.001235	7.012301	**4.978995**
Img3	6.454673	5.945612	7.124512	**5.012354**

The results show that the experimental results in the river are similar to those in the strong turbulence environment, but in the ocean, they are more similar to those in the micro turbulence environment. Therefore, the effectiveness of the experimental results in the river is similar to that in the strong turbulence environment, and in the ocean environment, the micro turbulence is more similar. In this case, the validity of the laboratory experiments and the reliability of the proposed algorithm can be verified. And from table 6, this method is obviously better than other methods in regards to the algorithm running time, reflecting the advantages of real-time applications.

IV. CONCLUSION

Based on the idea of deep learning, an improved deep-intensive convolution neural network is proposed in this paper. The main innovation is that the wavelet basis is introduced into the deep learning convolution kernel based on the turbulence structure, and an improved dense block structure is proposed. The experimental results show that, when there is reference image, the value of PSNR and SSIM is effectively improved; when there is no reference image, the values of BM, GMG and LS are also improved. Therefore, it can be concluded that the proposed method can effectively improve the effect of depth neural network in the super resolution reconstruction of imaging in turbulent water.

However, it is undeniable that the training set used in this method is based on underwater images, so its extensibility needs to be studied. Therefore, the next step should focus on studying the applicability of this method in other fields to improve the universality of this method.

REFERENCES

[1] Y. Chen and K. Yang, "MAP-regularized robust reconstruction for underwater imaging detection," *Optik*, vol. 124, no. 20, pp. 4514–4518, Oct. 2013.
[2] X. Yang, H. Mei, J. Zhang, K. Xu, B. Yin, Q. Zhang, and X. Wei, "DRFN: Deep recurrent fusion network for single-image super-resolution with large factors," *IEEE Trans. Multimedia*, vol. 21, no. 2, pp. 328–337, Feb. 2019.
[3] J. Kim, J. K. Lee, and K. M. Lee, "Accurate image super-resolution using very deep convolutional networks," in *Proc. IEEE Conf. Comput. Vis. Pattern Recognit. (CVPR)*, Jun. 2016, pp. 1646–1654.
[4] J. Kim, J. K. Lee, and K. M. Lee, "Deeply-recursive convolutional network for image super-resolution," in *Proc. IEEE Conf. Comput. Vis. Pattern Recognit. (CVPR)*, Jun. 2016, pp. 1637–1645.
[5] X. Fu, Z. Fan, M. Ling, Y. Huang, and X. Ding, "Two-step approach for single underwater image enhancement," in *Proc. Int. Symp. Intell. Signal Process. Commun. Syst. (ISPACS)*, Xiamen, China, Nov. 2017, pp. 789–794.
[6] P. L. J. Drews, E. R. Nascimento, S. S. C. Botelho, and M. F. M. Campos, "Underwater depth estimation and image restoration based on single images," *IEEE Comput. Graph. Appl.*, vol. 36, no. 2, pp. 24–35, Mar. 2016.
[7] C.-Y. Li, J.-C. Guo, R.-M. Cong, Y.-W. Pang, and B. Wang, "Underwater image enhancement by dehazing with minimum information loss and histogram distribution prior," *IEEE Trans. Image Process.*, vol. 25, no. 12, pp. 5664–5677, Dec. 2016.
[8] Y.-T. Peng and P. C. Cosman, "Underwater image restoration based on image blurriness and light absorption," *IEEE Trans. Image Process.*, vol. 26, no. 4, pp. 1579–1594, Apr. 2017.
[9] C. Ancuti, C. O. Ancuti, T. Haber, and P. Bekaert, "Enhancing underwater images and videos by fusion," in *Proc. IEEE Conf. Comput. Vis. Pattern Recognit.*, Providence, RI, USA, Jun. 2012, pp. 81–88.
[10] A. S. Abdul Ghani and N. A. Mat Isa, "Underwater image quality enhancement through integrated color model with Rayleigh distribution," *Appl. Soft Comput.*, vol. 27, pp. 219–230, Feb. 2015.
[11] C. Li, J. Guo, C. Guo, R. Cong, and J. Gong, "A hybrid method for underwater image correction," *Pattern Recognit. Lett.*, vol. 94, pp. 62–67, Jul. 2017.
[12] C. Li, J. Guo, and C. Guo, "Emerging from water: Underwater image color correction based on weakly supervised color transfer," *IEEE Signal Process. Lett.*, vol. 25, no. 3, pp. 323–327, Mar. 2018.
[13] X. Sun, L. Liu, Q. Li, J. Dong, E. Lima, and R. Yin, "Deep pixel-to-pixel network for underwater image enhancement and restoration," *IET Image Process.*, vol. 13, no. 3, pp. 469–474, Feb. 2019.
[14] H. Lu, Y. Li, T. Uemura, H. Kim, and S. Serikawa, "Low illumination underwater light field images reconstruction using deep convolutional neural networks," *Future Gener. Comput. Syst.*, vol. 82, pp. 142–148, May 2018.
[15] X. Sun, L. Liu, and J. Dong, "Underwater image enhancement with encoding-decoding deep CNN networks," in *Proc. IEEE SmartWorld, Ubiquitous Intell. Comput., Adv. Trusted Comput., Scalable Comput. Commun., Cloud Big Data Comput., Internet People Smart City Innov. (SmartWorld/SCALCOM/UIC/ATC/CBDCom/IOP/SCI)*, San Francisco, CA, USA, Aug. 2017, pp. 4–8.
[16] W. Hou, Z. Lee, and A. D. Weidemann, "Why does the Secchi disk disappear? An imaging perspective," *Opt. Express*, vol. 15, no. 6, pp. 2791–2802, 2007.
[17] W. Hou, D. J. Gray, A. D. Weidemann, and R. A. Arnone, "Comparison and validation of point spread models for imaging in natural waters," *Opt. Express*, vol. 16, no. 13, pp. 9958–9965, Jun. 2008.
[18] W. Hou, "A simple underwater imaging model," *Opt. Lett.*, vol. 34, no. 17, pp. 2688–2690, 2009.
[19] W. Hou, E. Jarosz, S. Woods, W. Goode, and A. Weidemann, "Impacts of underwater turbulence on acoustical and optical signals and their linkage," *Opt. Express*, vol. 21, no. 4, pp. 4367–4375, 2013.
[20] W. Hou, S. Woods, E. Jarosz, W. Goode, and A. Weidemann, "Optical turbulence on underwater image degradation in natural environments," *Appl. Opt.*, vol. 51, no. 14, pp. 2678–2686, 2012.

[21] G. Nootz, W. Hou, F. R. Dalgleish, and W. T. Rhodes, "Determination of flow orientation of an optically active turbulent field by means of a single beam," *Opt. Lett.*, vol. 38, no. 13, pp. 2185–2187, 2013.
[22] G. Nootz, E. Jarosz, F. R. Dalgleish, and W. Hou, "Quantification of optical turbulence in the ocean and its effects on beam propagation," *Appl. Opt.*, vol. 55, no. 31, pp. 8813–8820, 2016.
[23] G. Nootz, S. Matt, A. Kanaev, K. P. Judd, and W. Hou, "Experimental and numerical study of underwater beam propagation in a Rayleigh–Bénard turbulence tank," *Appl. Opt.*, vol. 56, no. 22, pp. 6065–6072, 2017.
[24] S. Matt, W. Hou, S. Woods, W. Goode, E. Jarosz, and A. Weidemann, "A novel platform to study the effect of small-scale turbulent density fluctuations on underwater imaging in the ocean," *Methods Oceanogr.*, vol. 11, pp. 39–58, Dec. 2014.
[25] S. Matt, W. Hou, W. Goode, and S. Hellman, "Introducing SiTTE: A controlled laboratory setting to study the impact of turbulent fluctuations on light propagation in the underwater environment," *Opt. Express*, vol. 25, no. 5, pp. 5662–5683, 2017.
[26] N. Farwell and O. Korotkova, "Intensity and coherence properties of light in oceanic turbulence," *Opt. Commun.*, vol. 285, no. 6, pp. 872–875, Mar. 2012.
[27] N. H. Farwell and O. Korotkova, "Multiple phase-screen simulation of oceanic beam propagation," *Proc. SPIE, Int. Soc. Opt. Eng.*, vol. 9224, Oct. 2014, Art. no. 922416.
[28] H. Shen, M. K. Ng, P. Li, and L. Zhang, "Super-resolution reconstruction algorithm to MODIS remote sensing images," *Comput. J.*, vol. 52, no. 1, pp. 90–100, Feb. 2008.
[29] H. Shen, L. Zhang, B. Huang, and P. Li, "A MAP approach for joint motion estimation, segmentation, and super resolution," *IEEE Trans. Image Process.*, vol. 16, no. 2, pp. 479–490, Feb. 2007.
[30] H. Shen, L. Peng, L. Yue, Q. Yuan, and L. Zhang, "Adaptive norm selection for regularized image restoration and super-resolution," *IEEE Trans. Cybern.*, vol. 46, no. 6, pp. 1388–1399, Jun. 2016.
[31] B. Lim, S. Son, H. Kim, S. Nah, and K. M. Lee, "Enhanced deep residual networks for single image super-resolution," in *Proc. IEEE Conf. Comput. Vis. Pattern Recognit. Workshops (CVPRW)*, Jul. 2017, pp. 136–144.
[32] X. Wang, K. Yu, C. Dong, and C. Change Loy, "Recovering realistic texture in image super-resolution by deep spatial feature transform," in *Proc. IEEE/CVF Conf. Comput. Vis. Pattern Recognit. (CVPR)*, Jun. 2018, pp. 606–615.
[33] W. Zhang, Y. Liu, C. Dong, and Y. Qiao, "RankSRGAN: Generative adversarial networks with ranker for image super-resolution," in *Proc. IEEE/CVF Int. Conf. Comput. Vis. (ICCV)*, Oct. 2019, pp. 3096–3105.
[34] Y. Chen and J. Chen, "Spatial adaptive regularized MAP reconstruction for LD-based night vision," *Optik*, vol. 125, no. 13, pp. 3162–3165, 2014.
[35] Y. Chen, W. Yang, H. Tan, Y. Yang, N. Hao, and K. Yang, "Image enhancement for LD based imaging in turbid water," *Optik*, vol. 127, no. 2, pp. 517–521, Jan. 2016.
[36] A. Duarte, F. Codevilla, J. D. O. Gaya, and S. S. C. Botelho, "A dataset to evaluate underwater image restoration methods," in *Proc. OCEANS Shanghai*, Shanghai, China, Apr. 2016, pp. 1–6.

YUZHANG CHEN was born in 1984. He received the bachelor's, master's, and Ph.D. degrees from the Huazhong University of Science and Technology. He is currently an Associate Professor and a Master Tutor with the School of Computer and Information Engineering, Hubei University. He has been engaged in research on photoelectric imaging detection, photoelectric information perception, image processing, and embedded development for a long time. His main research contents include laser and LED in water, night vision or underwater scattering medium radiation transmission theory and computer simulation, image acquisition and restoration and reconstruction algorithms, and image processing algorithms embedded including the research of android development.

KANGLI NIU is currently pursuing the degree in electronic information engineering with the School of Computer and Information Engineering, Hubei University. His main research directions are image processing and computer vision. At present, he has done a lot of research on image recognition and processing in the laboratory, and accumulated a lot of professional knowledge and experimental experience.

ZHANGFAN ZENG received the B.S., M.S., and Ph.D. degrees from Wuhan University, China, The University of Manchester, U.K., and the University of Birmingham, U.K., in 2006, 2007, and 2013, respectively, all in communication engineering. Since December 2015, he has been a full-time Associated Professor with Hubei University, China. He has published over 20 research articles and one patent in radar community. His research areas are wireless communication and digital signal processing.

YONGCAI PAN (Fellow, IEEE) is currently a Full Professor and the Head of the Laboratory of Signal Processing and System Analysis, Hubei University. His research areas include wireless communication, signal processing, and intelligent systems. He has extensive exposure and experience in industrial projections.